Journal of Solid State Chemistry 184 (2011) 264–272

Contents lists available at ScienceDirect

Journal of Solid State Chemistry

journal homepage: www.elsevier.com/locate/jssc

Preparation, characterization, magnetic susceptibility (Eu, Gd and Sm) and XPS studies of Ln_2ZrTiO_7 (Ln=La, Eu, Dy and Gd)

B. Vijaya Kumar [a], Radha Velchuri [a], V. Rama Devi [a], B. Sreedhar [b], G. Prasad [c], D. Jaya Prakash [d], M. Kanagaraj [e], S. Arumugam [e], M. Vithal [a,*]

[a] Department of Chemistry, Osmania University, Hyderabad 500 007, India
[b] Inorganic and Physical Chemistry Division, Indian Institute of Chemical Technology, Hyderabad 500 007, India
[c] Department of Physics, Osmania University, Hyderabad 500 007, India
[d] College of Technology, Osmania University, Hyderabad 500 007, India
[e] Centre for High Pressure Research, School of Physics, Bharathidasan University, Tiruchirapalli 620 024, India

ARTICLE INFO

Article history:
Received 1 July 2010
Received in revised form
6 November 2010
Accepted 9 November 2010
Available online 18 November 2010

Keywords:
Sol–gel
Raman
Magnetic susceptibility
XPS

ABSTRACT

Bulk and nanosized pyrochlore materials Ln_2ZrTiO_7 (Ln=La, Eu, Dy, Gd and Sm) have been prepared by the sol–gel method. All the samples were characterized by powder X-ray diffraction, Raman and X-ray photoelectron spectroscopy. Magnetic susceptibility (χ) measurements of Gd_2ZrTiO_7, Sm_2ZrTiO_7 and Eu_2ZrTiO_7 were carried out by vibrating sample magnetometer in the temperature range 2–320 K. The variation of χ^{-1} (or χ) with temperature of Gd_2ZrTiO_7, Sm_2ZrTiO_7 and Eu_2ZrTiO_7 follows the Curie law, intermediate formula and the Curie–Weiss law, respectively. From the linear portion of χT vs. T^{-1} plot of Eu_2ZrTiO_7 from 2 to 15 K, the classical nearest neighbor exchange (J^{cl}) and dipolar interactions (D_{nn}) are obtained. The XPS of Ln_2ZrTiO_7 (Ln=La, Eu, Dy and Gd) gave characteristic peaks for Ln, Ti, Zr and O. The satellite peaks are observed only for 3*d* La of La_2ZrTiO_7.

1. Introduction

The general formula of pyrochlore oxides is $A_2B_2O_7$ or more appropriately written as $A_2B_2O_6O'$ to indicate B_2O_6 network intersecting with A–O′ cations of formula A_2O' [1]. These oxides crystallize in cubic lattice with space group $Fd\bar{3}m$. Cation "*A*" can be a trivalent rare earth or divalent alkaline earth or monovalent alkali ions. Cation "*B*" will be a 3*d*, 4*d* or 5*d* transition metal ion of appropriate oxidation state for charge neutrality. The larger "*A*" cation with eight fold coordination occupies 16*d* position while smaller "*B*" cation with six fold coordination occupies 16*c* position. In pyrochlore structure all the oxygens are tetrahedrally coordinated but not equivalent. They occupy 48*f*, 8*a* and 8*b* positions. The oxygen ions on the 48*f* which are bonded to two *A* cations and two B cations while the oxygen ions on 8*a* are bonded to four *B* ions. The site 8*b* is surrounded by four *A* cations. It should be noted that the 8*a* would be vacant if 16*c* position is taken as origin (000) [1]. Oxygen defects can also occur in the A_2O' network. Thus the structure is flexible for substitution at *A* or *B* sites giving rise to a large family of materials. The pyrochlore structure is closely related to defect fluorite structure. The unit cell parameters of pyrochlore are twice to that of defect fluorite. The stability of pyrochlore materials was found to depend on the r_A/r_B (r=radius) ratio. The upper and lower limits of this ratio were found to be 1.7 and 1.2, respectively. Materials whose radius ratio is close to 1.2 were found to crystallize in defect fluorite while those with ratio close to 1.7 crystallize in ordered pyrochlore. It should be noted that the numerical value of radius ratio r_A/r_B is used only as a broad guide line in view of some exceptions [2]. Pyrochlore oxides are used as materials for immobilization of actinide-rich wastes [3,4], as electrolytes in solid state fuel cells [5], as combustion catalysts [6], as chemical sensors [7]. These materials exhibit variable ionic and electronic conductivity which is related to cation (*A* and *B*) and oxygen anion vacancies [8–10]. For instance substitution of Zr in place of Ti in the $Gd_2(Ti_{1-x}Zr_x)_2O_7$ system results a two-order increase in the ionic conductivity which is related to an increase in the anion disorder [9]. Further, pyrochlore oxides containing rare earth ions exhibit remarkable X-ray photoelectron spectral features and interesting emission properties. The 4*f* levels in rare earth ions (except Ce) are strongly localized within the ion and their contribution to chemical bonding is insignificant, the exception being Mott-type phase transition of Pr in metallic systems under pressure [11,12]. The observation of satellite peaks for 3*d* core level in the XPS spectra of rare earth ions and their interpretation makes these rare earth titanium pyrochlores worthy of investigations.

The structure of $Ln_2M_2O_7$ (Ln=rare earth and M=Ti^{4+} or Zr^{4+}) is characterized by corner shared MO_6 octahedra forming M_2O_6 network which intersects with Ln–O′ chains of formula Ln_2O' [1]. Such an

* Corresponding author. Fax: +91 40 27090020.
E-mail address: muga_vithal@osmania.ac.in (M. Vithal).

0022-4596/$ - see front matter © 2010 Elsevier Inc. All rights reserved.
doi:10.1016/j.jssc.2010.11.014

arrangement of magnetic metal ions (Ln^{3+} ions, as Ti^{4+} or Zr^{4+} being nonmagnetic) prevents the possibility of obtaining all the pairwise spin–spin interactions simultaneously. This leads to frustration of interactions among the rare earth (Ln) ions and is known as geometrical frustration (GF). In addition to this, the crystal field influences the rare earth ion producing single ion anisotropy (SIA) leading to interesting magnetic properties. It is observed that nearest-neighbor exchange (J_{nn}) and dipolar interactions (D_{nn}) together with SIA influence the GF properties considerably at low temperatures. Geometrically frustrated titanate pyrochlores of composition $Ln_2Ti_2O_7$ have been extensively studied owing to their novel properties such as spin-ice behavior in $Dy_2Ti_2O_7$ and $Ho_2Ti_2O_7$ [13,14] and spin-liquid state in $Tb_2Ti_2O_7$ [15]. Systems such as $Er_2Ti_2O_7$, $Yb_2Ti_2O_7$ and $Gd_2Ti_2O_7$ exhibit planar magnetism ($\chi_{\perp} \gg \chi_{\parallel}$) at low temperature and considered as "*XY*" pyrochlores. The spins of Er^{3+} and Yb^{3+} fluctuate considerably leading to the phenomena of order by disorder (in $Er_2T_{i2}O_7$) [16] and quantum fluctuation regime (in $Yb_2Ti_2O_7$) [17]. Further, these materials were found to exhibit mixed conductivity, giant magneto resistance, piezoelectric behavior, high chemical stability against radiation damage, ferromagnetism and ferrimagnetism [1,8,14,15,18,19]. Although majority of rare earth titanate pyrochlore oxides exhibit ant ferromagnetic type interactions (except $Yb_2Ti_2O_7$ which shows ferromagnetic interactions), the dipolar and spin fluctuations together with on site anisotropy of lanthanide ions result in unusual magnetic properties. Furthermore, the energy difference between ground state and first excited state of lanthanide ions (like Sm^{3+} and Eu^{3+}), which is comparable to thermal energy, k_bT, also leads to interesting magnetic properties. To our knowledge, the magnetic properties of Gd_2ZrTiO_7, Sm_2ZrTiO_7 and Eu_2ZrTiO_7 are not reported. In the present investigation, we report the magnetic susceptibility (of bulk Gd_2ZrTiO_7, Sm_2ZrTiO_7 and Eu_2ZrTiO_7) along with preparation, characterization and XPS studies of Ln_2ZrTiO_7 (*Ln* = La, Eu Dy and Gd). The powder XRD, Raman, conductivity and XPS studies of Gd_2ZrTiO_7 and conductivity studies of Dy_2ZrTiO_7 are reported earlier [9,20,21]. The preparation of Sm_2ZrTiO_7 (SZT), powder XRD, Raman and its XPS studies were reported earlier [22]. The compositions La_2ZrTiO_7, Sm_2ZrTiO_7, Eu_2ZrTiO_7, Dy_2ZrTiO_7 and Gd_2ZrTiO_7 are abbreviated as LZT, SZT, EZT, DZT and GZT, respectively. The abbreviation followed by a three digit number refers to the temperature at which the material is obtained. For instance, LZT-700 stands for La_2ZrTiO_7 prepared at 700 °C.

2. Experimental

2.1. Materials

Rare earth oxide (Ln_2O_3, *Ln* = La, Eu, Dy and Gd) (Indian Rare Earths Ltd., purity 99%), zirconyl nitrate (Wilson Laboratories, Bombay), Titanium powder (100 mesh, Aldrich 99.7%), H_2O_2 (30%, SD Fine) and ammonia solution (25%, AR grade, SD Fine) were used as received.

2.2. Preparation of Ln_2ZrTiO_7

Solution "*A*": stoichiometric amount of Ln_2O_3 was dissolved in excess concentrated HNO_3 to form rare earth nitrate. Excess nitric acid was removed by slow heating. About 25 ml of distilled water was added. Solution "*B*": calculated amount of zirconyl nitrate was dissolved in hot water. Solution "*C*": stoichiometric amount of Ti powder was added to a solution containing 60 ml of H_2O_2 and 10 ml of ammonia at 0–10 °C under constant stirring. A yellow gel was obtained after 6 h. Solution "*A*" was mixed with solution "*B*". To this resultant solution, solution "*C*" was added. Then citric acid was added to this solution such that the mole ratio of citric acid: metal ion is 2:1. At this stage metal citrates are believed to be formed. The total volume of the solution was about 300 ml. The pH of the resultant metal citrate solution was adjusted to 6–7 by adding dilute ammonia solution dropwise. The solution was then slowly evaporated on a water bath till a viscous liquid was obtained. At this stage ethylene glycol (gelating reagent) was added such that the molar ratio of citric acid to ethylene glycol is 1:1.2. This mixture was heated on a hot plate/stirrer at 100 °C for 2–3 h with constant stirring. The temperature was increased to 160–180 °C at the onset of solidification. The ensuing porous solid mass was ground in an agate mortar using spectral grade acetone and heated at 400 °C in small amounts in an electric burner to remove the organic matter completely. The resultant ash color solid (named as "precursor") was heated in a muffle furnace at various temperatures (500–900 °C) for 5 h.

2.3. Characterization

The powder X-ray diffractograms were recorded on Siemens D-5000 powder X-ray diffract meter using Cu*K*α radiation of wavelength 1.5406 Å. SEM-EDS were recorded on the HITACHI SU-1500 variable pressure scanning electron microscope (VP-SEM). Raman spectra were recorded using a 632.81 nm line from a He–Ne laser and the scattered light was analyzed using HORIBA JOBIN YVON HR800. The laser was focused to a spot of ~3 μm and a 10 × lens was used for the collection of back scattered Raman signal. UV–vis diffuse reflectance spectra (DRS) of the samples were recorded using Perkin Elmer Lamda 750 UV–vis spectrometer in the 200–1100 nm range. Room temperature ESR spectra were recorded on a JOEL PE-3X, X-band spectrometer equipped with a 100 kHz field modulation unit. The ESR spectrometer was optimized for modulation amplitude receiver gain, time constant and scans time. X-ray photoelectron spectroscopic (XPS) measurements were performed on a KRATOS AXIS165 X-ray photoelectron spectrometer using excitation energy of 1253.6 eV (Mg*K*α), the spectra were recorded with pass energy of 80 eV. The temperature dependence of dc magnetic susceptibility measurements were performed by 9 T vibrating sample magnetometer (Quantum Design, USA) with applied magnetic field of 1 T.

3. Results and discussion

3.1. Powder X-ray diffraction

The precursors of LZT, EZT, DZT and GZT are calcined at 400, 500, 600, 700, 800 and 900 °C separately for 5 h each. The precursors of all the compounds calcined at 400 °C, which were black in color, gave no diffraction lines in the powder pattern indicating the absence of long range order. The powder XRD of LZT-500 and LZT-600 were characterized by broad background with the appearance of peaks in the 2θ range 28–35°, 46–50° and 55–62°. The presence of broad base line at these temperatures indicates the amorphous nature of the samples along with some crystalline phase. The powder XRD of LZT-700 clearly shows the phase formation. All the observed peaks of LZT-700, LZT-800 and LZT-900 are broad indicating the nanonature of the materials. Unlike LZT, the crystallization of EZT was found to be above 700 °C which is higher than the crystallization temperatures observed in other related rare earth pyrochlore systems. It could be due to the nature of the sample. The powder XRDs of EZT-800 and EZT-900 clearly show the complete phase formation with typical line broadening indicating the nanonature of the materials. The powder XRD of DZT-600 clearly shows the typical pattern expected for a pyrochlore type material. The crystallization of DZT is in the range 500–600 °C. The crystallite size obtained from the full width at half maximum of intense XRD line using Scherrer's formula for LZT, EZT and DZT samples is shown in Table 1. The powder XRD pattern of GZT is similar to that reported earlier for $Gd_2Ti_2O_7$ [23]. The powder XRD

Table 1
Crystallite size of LZT, EZT and DZT powders calcined at different temperatures.

Compound	Temperature (°C)/5 h	Crystallite size (nm)
LZT	700	13.8
	800	14.6
	900	16.7
EZT	700	5.6
	800	7.2
	900	20.6
DZT	700	8.3
	800	11.2
	900	13.8

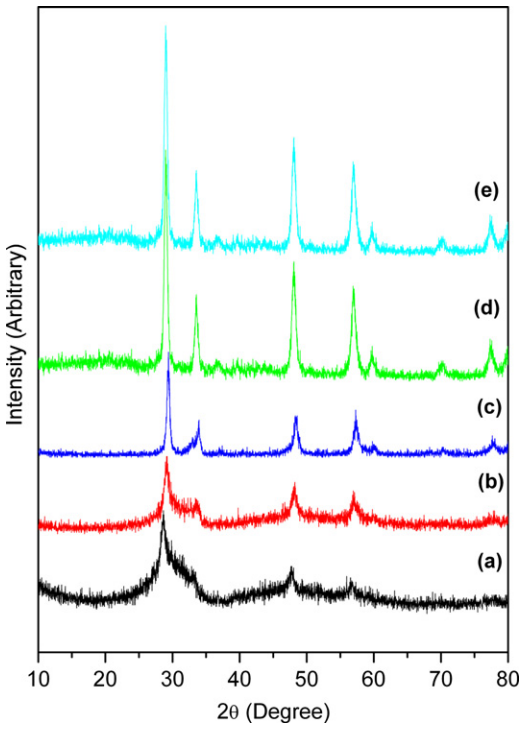

Fig. 1. Powder XRD patterns of LZT precursor calcined at (a) 500 °C, (b) 600 °C, (c) 700 °C (d) 800 °C and (e) 900 °C.

patterns of LZT and DZT are similar to each other and similar to $La_2Zr_2O_7$ and $Dy_2Ti_2O_7$, respectively [24,25]. It is well known that the $A_2B_2O_7$ types of compounds crystallize in (i) ordered pyrochlore or (ii) disordered pyrochlore or (iii) defect fluorite structure, all having cubic lattice. The unit cell length (a) is about 5 Å for defect fluorite structure while for ordered and disordered pyrochlores the unit cell length is about 10 Å. It is noticed that in ordered pyrochlore structure, super lattice peaks at $2\theta \approx 14°$, 27°, 36° and 50° (for Cu$K\alpha$ source) for (111), (311), (331) and (531) planes, respectively, are observed [2]. If $A_2B_2O_7$ adopts defect fluorite structure, these super lattice peaks will be absent in its powder XRD pattern. Very often the intensity of super lattice peaks will be too small to the observed and laboratory X-ray diffractometer may not detect them. Thus it can be concluded that observation of super lattice peaks confirm the ordered pyrochlore structure for the material but converse may not be true. In Figs. 1–3, the observed XRD patterns of LZT, EZT and DZT are shown. The unit cell parameters of LZT, EZT and DZT are found to be 10.76, 10.36 and 10.38 Å, respectively. It is noticed that the unit cell parameter decreases from LZT ($r_{La^{3+}} = 1.18$) to EZT ($r_{Eu^{3+}} = 1.07$). The variation in the unit cell parameter from EZT to DZT ($r_{Dy^{3+}} = 1.03$) is not significant probably due to almost similar sizes of Eu^{3+} and Dy^{3+}.

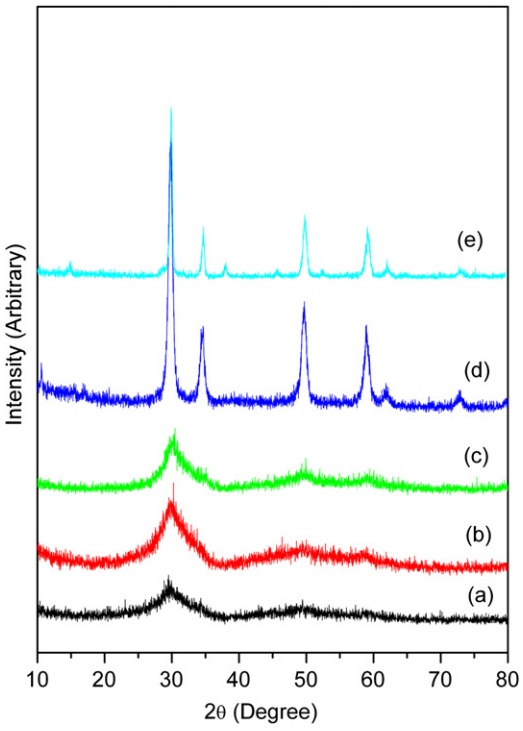

Fig. 2. Powder XRD patterns of EZT precursor calcined at (a) 500 °C, (b) 600 °C, (c) 700 °C (d) 800 °C and (e) 900 °C.

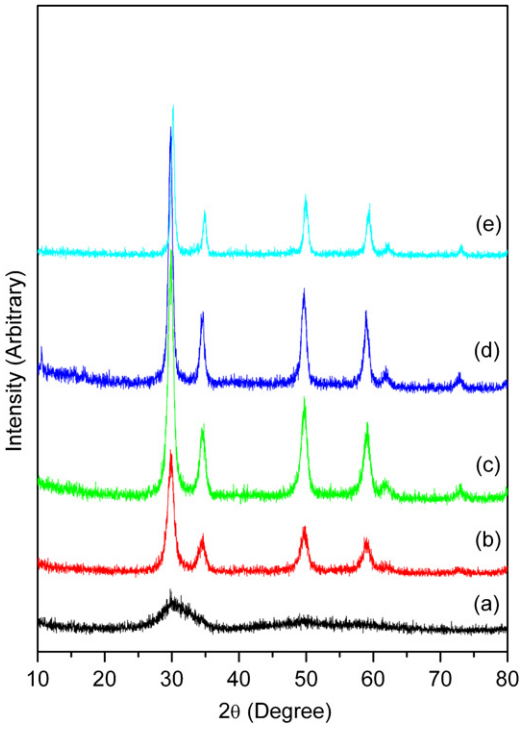

Fig. 3. Powder XRD patterns of DZT precursor calcined at (a) 500 °C, (b) 600 °C, (c) 700 °C (d) 800 °C and (e) 900 °C.

A close examination of powder XRDs of LZT and EZT shows the presence of weak super lattice peaks and hence expected to crystallize in ordered pyrochlore lattice. In the case of DZT the super lattice peaks are not observed in the powder XRD. DZT may be a "weakly ordered" pyrochlore structure as its Raman spectrum

is intermediate to "ordered pyrochlore" and "defect fluorite" structures. This is further elaborated while discussing the Raman spectra. Dickson et al. have shown that the numerical value of *x*, the positional parameter of 48*f* oxygen, gives information regarding the type of structure (ordered pyrochlore/disordered pyrochlore/defect fluorite) adopted by $A_2B_2O_7$ type oxides [26].

3.2. EDS analysis

The energy dispersive spectra of all the samples prepared at 900 °C are recorded. The area ratio of Ln, Zr and Ti was found to be close to 2:1:1 confirming the molecular formula as Ln_2ZrTiO_7. The atomic percentage of Ln, Zr and Ti for all the samples is shown in Table 2.

Table 2
Atom percentage of Ln:Zr:Ti for Ln_2ZrTiO_7 series.

Atom percentage	LZT	EZT	DZT	GZT
O, K	66.03	64.09	61.66	67.10
Ti, K	8.05	9.21	9.72	8.37
Zr, L	9.44	8.77	8.93	8.40
Ln	16.48	17.93	19.69	16.13

3.3. Raman spectra

Raman spectroscopic investigation gives unequivocal information regarding the structure adopted by $A_2B_2O_7$ materials. The Raman spectra of all the compounds calcined at different temperatures (500, 700 and 900 °C) were recorded. According to group theory analysis, $A_2B_2O_7$ oxides crystallized in ordered pyrochlore and defect fluorite structures give six and one Raman active modes, respectively [27]:

$\Gamma = A_{1g} + E_g + 4F_{2g}$ (for ordered pyrochlore)

$\Gamma = F_{2g}$ (for defect fluorite)

The Raman spectra of all the compounds calcined at 500 °C gave a straight line without any spectral characteristic peaks observed for pyrochlore oxides. Hence compounds calcined at 500 °C are truly amorphous. The Raman spectra of LZT, EZT, DZT and GZT compounds calcined at 700 °C (figure not given) gave broad bands. The broad bands were fitted to six Lorentzians. The Raman spectra of LZT, EZT and DZT calcined at 900 °C were collected in Fig. 4a, b, c, respectively. These Raman spectra are similar to those reported earlier [28] for pyrochlore oxides. Thus LZT, EZT, DZT and GZT have also crystallized in "pyrochlore" structure. The broadness of the Raman spectra is probably due to (a) small crystallite size and/or (b) cation disorder in the system. In LZT sample, the most intense

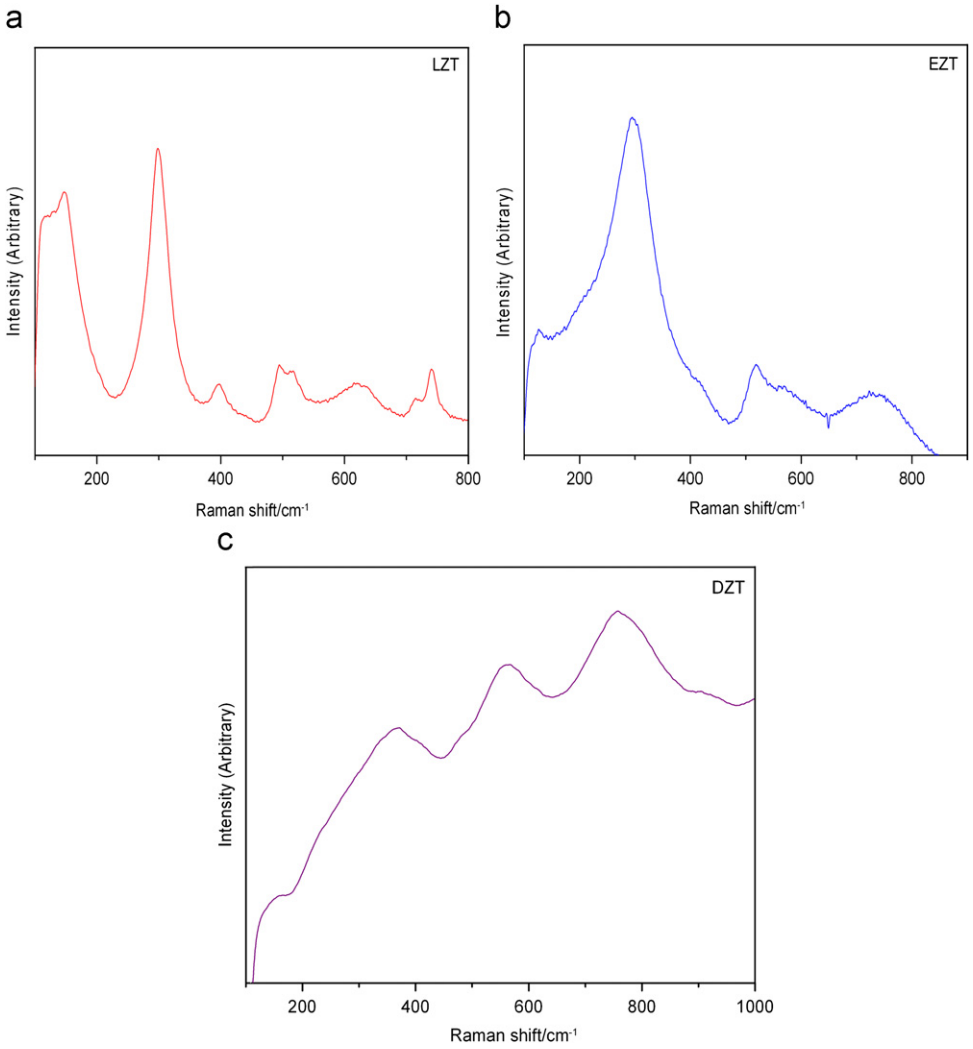

Fig. 4. Raman spectra of (a) LZT, (b) EZT and (c) DZT.

Table 3
Raman peak positions (in cm^{-1}) and their assignments of LZT, EZT, DZT and GZT calcined at 900 °C along with the peak positions of related systems.

LZT	EZT	DZT	GZT	$Gd_2Ti_2O_7$ [28]	Assignment
519	520	560	–	519	F_{2g}/A_{1g}
300	300	360	320	312	E_g
148	128	153	130	219	F_{2g}
400	–	–	–	455	F_{2g}
620	–	–	586	549	F_{2g}
740	730	750	740	–	Combination band

peak observed at 300 cm^{-1} was assigned to E_g while less intense peaks at 148, 400, 519 and 620 cm^{-1} were assigned to four F_{2g} modes. The band observed at 740 cm^{-1} may be assigned to a combination band as reported earlier [27]. Although the Raman spectrum of DZT is similar to that of LZT and EZT, it shows a shift in the positions of the bands and a decrease in intensity of E_g band. Mandal et al. have reported the Raman spectra of $RE_2Hf_2O_7$ (RE=Dy, Ho, Err, Tm, Lu and Y) [2]. They have noticed that the Raman spectrum of $Dy_2Hf_2O_7$ can be compared with other ordered pyrochlores $RE_2Hf_2O_7$ (RE=Dy, Ho, Err, Tm, Lu and Y), but is not a truly ordered pyrochlore. $Dy_2Hf_2O_7$ has a tendency to form pyrochlore structure. The Raman spectrum of DZT is similar with that of $Dy_2Hf_2O_7$ and hence can be classified as "weakly ordered" pyrochlore. The Raman results of DZT are in accordance with its powder XRD results. The Raman peak positions and their assignments of LZT, EZT, DZT and GZT are shown in Table 3 along with the peak positions of related systems [28]. The line widths of intense peak (E_g) for LZT, EZT, DZT and GZT (at 900 °C) were found to be ≈ 41, 84, 57 and 98 cm^{-1}, respectively. The magnitude of these line widths are higher than the line width found for bulk ordered pyrochlore materials. In the present investigation, the relatively broad line width in the Raman spectra is attributed to the both cation disorder and small crystallite size.

3.4. Diffuse reflectance spectra of DZT

Diffuse reflectance spectra of DZT (representative of the series LnZT) were recorded to characterize the nature (bulk/nano) of the samples and to estimate the band gap energy (E_g). Fig. 5(A) shows the diffuse reflectance spectra of DZT in the UV–visible region. DZT calcined at all temperatures exhibit absorption below 350 nm. The sample heated at 900 °C shows a shoulder in the 400–370 nm region. A systematic shift in the absorption edge to longer wavelength is noticed with increase in the calcination temperature. For a given oxide the absorption edge is strongly dependent on its crystallite size which is attributed to quantum size effects [29]. Accurate band gap energy of semiconducting oxides can be obtained from the plot of $(\alpha h\nu)^{1/2}$ vs. $h\nu$ where α is absorption coefficient and $h\nu$ is photon energy. Extrapolation of linear portion of the plot to $(\alpha h\nu)^{1/2}=0$ (i.e. onto the x-axis) gives an estimation of band gap energy. For diffuse reflectance spectra, absorbance vs. photon energy also gives a reasonable estimation of band gap energy. The absorbance vs. photon energy plots for DZT samples are given in Fig. 5(B). The band gap energies are found to be 3.6, 3.5, 3.4, 3.1 and 2.8 for the samples calcined at 500, 600, 700, 800 and 900 °C, respectively. It is observed that E_g increases with decrease in crystallite size. This result is in accordance with quantum size effect for semiconducting oxides.

3.5. Magnetic susceptibility

3.5.1. Gd_2ZrTiO_7

The ground state of Gd^{3+} is $^8S_{7/2}$. The excited states are $^6P_{5/2}$ and $^6P_{7/2}$. The energy difference between ground and first excited state

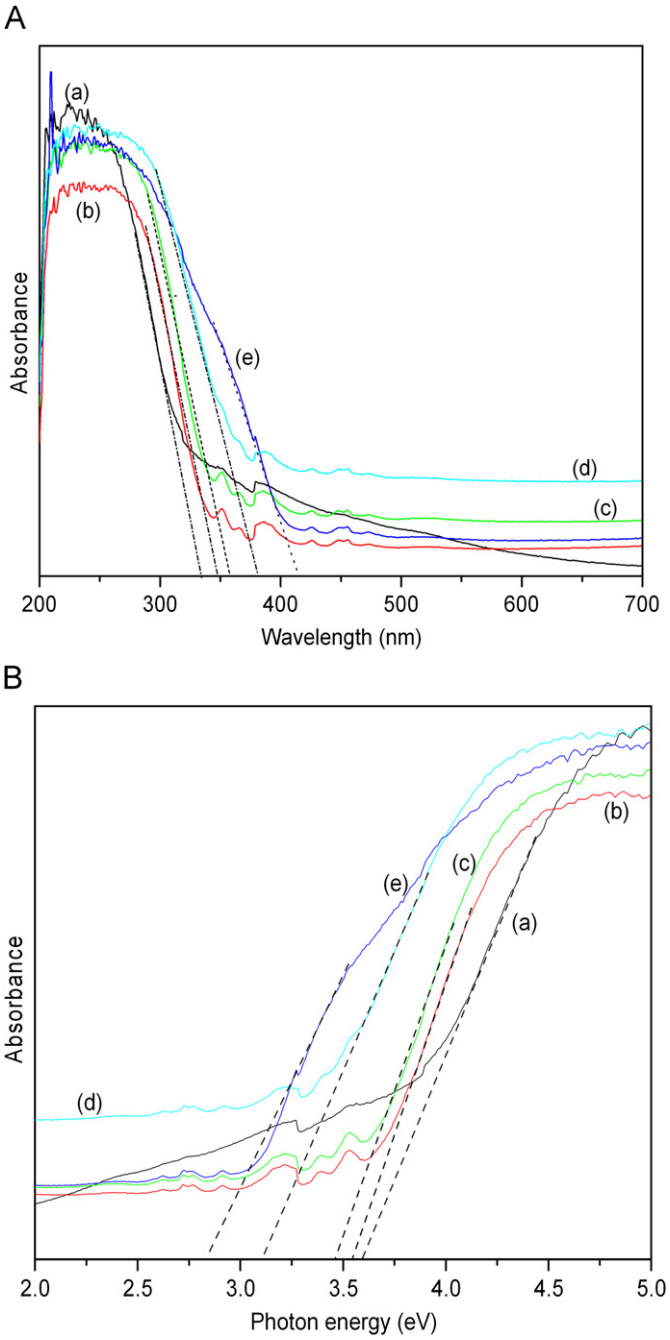

Fig. 5. (A) UV–vis diffuse reflectance spectra and (B) band gap energies of DZT calcined at (a) 500 °C, (b) 600 °C, (c) 700 °C, (d) 800 °C and (e) 900 °C.

is very large compare to the thermal energy, k_bT. At room temperature the populations in the excited states are negligible. Therefore, the magnetic properties of Gd^{3+} are due to its ground state populations only. It is well known that Gd^{3+} ions follow the Curie law over a wide range of temperatures, a characteristic feature of S state ions [30]. Fig. 6 shows the magnetic susceptibility (χ) vs. temperature (T) while χ^{-1} vs. T plot is shown in Fig. 7. The linear behavior of χ^{-1} vs. T plot shows the Curie nature of GZT. The effective magnetic moment calculated from the slope of χ^{-1} vs. T plot is found to be 7.6 BM which is lower than the free ion value expected for $4f^7$ configuration. The temperature coefficient $[-\chi^{-1}(d\chi/dT)]$ in the vicinity of 300 K is found to be (1/286) which is very close to theoretical value of (1/293) expected for Gd^{3+} ion and comparable with other Gd^{3+} systems [31]. The room

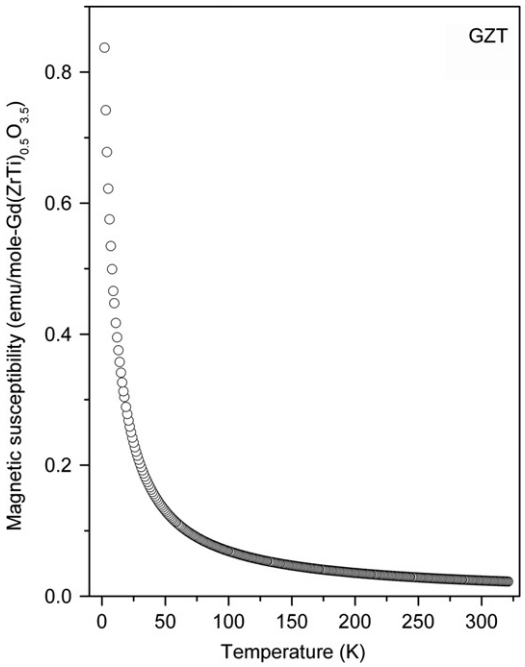

Fig. 6. Magnetic susceptibility vs. temperature of GZT.

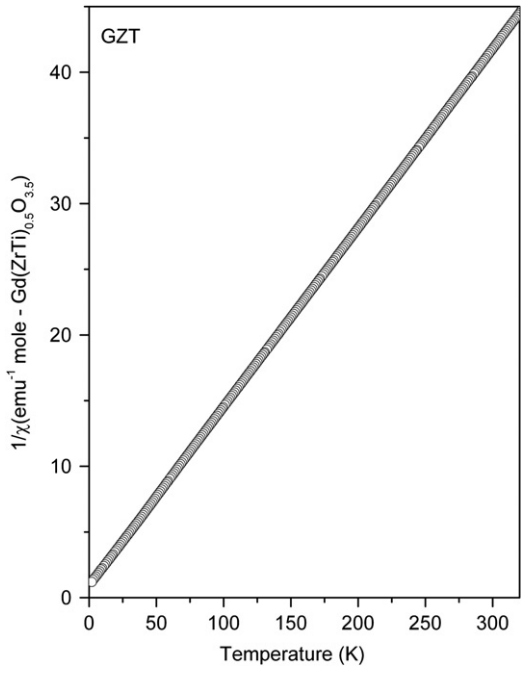

Fig. 7. Reciprocal magnetic susceptibility vs. temperature of GZT.

temperature X-band ESR spectrum shows a single broad line with $g=2.05$. The effective magnetic moment (μ_{eff}) calculated from ESR data is found to be 8.1 BM. The μ_{eff} from magnetic susceptibility and ESR data are found to be comparable within the experimental errors. These obtained values are close to the free ion value of 7.94 BM.

3.5.2. Sm_2ZrTiO_7

The ground state of Sm^{3+} is $^6H_{5/2}$ and its first excited state is $^6H_{7/2}$. The difference between these two energy levels is not infinitely large compared to thermal energy, k_bT. Therefore, the

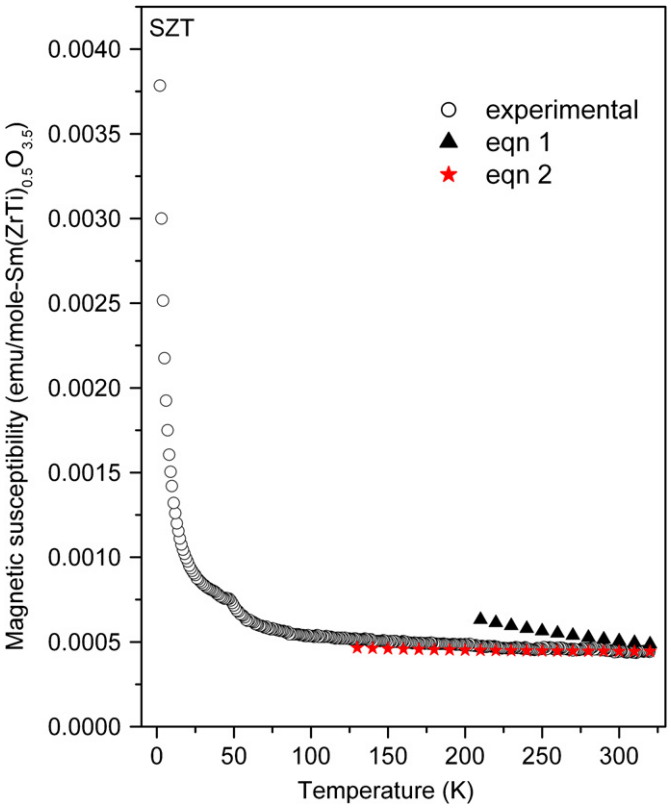

Fig. 8. Magnetic susceptibility vs. temperature of SZT.

populations in the first excited state become significant and invariably Sm^{3+} ion does not follow the simple Curie law or the Curie–Weiss law. Therefore, the magnetic susceptibility of SZT is fitted to an intermediate equation of the form [32]

$$\chi_{mol}(sm^{3+}) = \frac{C}{T}\frac{2.14+\frac{3.67}{\gamma}+\left(42.9+\frac{0.82}{\gamma}\right)e^{-7\gamma}+\left(142-\frac{0.33}{\gamma}\right)e^{-16\gamma}+\cdots}{3+4e^{-7\gamma}+5e^{-16\gamma}} \quad (1)$$

In this equation, $C=[N_A\mu_B^2/(3k_B)]$, where N_A and μ_B are the Avagadro number and the Bohr magneton, respectively. The parameter γ, is the ratio between the multiplet width and the thermal energy [$\gamma=\lambda/k_bT$]. Fig. 8 shows the magnetic susceptibility of SZT in the temperature range 2–320 K. The best fit using the above equation with $\lambda=500\ cm^{-1}$ is also shown in Fig. 8. It is observed that the line deviates from the experimental points at low temperatures probably due to the thickly populated ground state as the k_bT at low temperatures is very small compared to the energy difference between $^6H_{5/2}$ and $^6H_{7/2}$.

The susceptibility of Sm^{3+} can also be fitted in the high temperature region using

$$\chi_{mol}(Sm^{3+}) = \frac{C_1}{T}+\alpha_1+\frac{C_2}{T}e^{\Delta/T} \quad (2)$$

where Δ is the energy difference between the ground state ($^6H_{5/2}$), first excited state ($^6H_{7/2}$) and C_i ($i=1$ and 2) and α_1 are the Curie constant and the Van Vleck constant, respectively [30,32]. The parameters Δ and α_1 are related by $\alpha_1=1.07/\Delta$, when Δ is given in the Kelvin scale. The value of C_2 is fixed at 1.34 [30]. Using Eq. (2), the best fit to the experimental data in the temperature range 130–320 K is obtained for $\Delta=1741\ cm^{-1}$ and $C_1=0.005$ (Fig. 8). For Sm^{3+} ion, Δ is equal to 3.5λ, where λ is the spin–orbit coupling constant. Thus a value of 1741 cm^{-1} for Δ corresponds to $\lambda=497\ cm^{-1}$ which is in good agreement with the λ value obtained using Eq. (1). The effective magnetic moment is found to be $\mu_{eff}=0.768$

BM (at 300 K), which is smaller than the free ion moment of 1.3–1.4 BM. This may be because of the large crystal field splitting of the lowest $J=5/2$ multiplet. The μ_{eff} decreases to 0.25 BM at 2 K indicating the absence of magnetic ordering of Sm^{3+} spins presumably due to geometrical frustration of samarium spins. Similar observations are reported by Singh et al. [33].

3.5.3. Eu_2ZrTiO_7

The magnetic properties of Eu^{3+} compounds are unique among the rare earth compounds. The ground state of Eu^{3+} ($4f^6$) is nonmagnetic $^7F_0$. The first excited state is magnetic $^7F_1$ which is about 250–400 cm^{-1} above the ground state. This is followed by other excited terms $^7F_{2-6}$. At room temperature the thermal energy (k_bT) is ~210 cm^{-1} and the population in the first excited state becomes significant. Thus the observed magnetic properties of Eu^{3+} compounds are due to the relative populations in the ground and excited states. The variation of magnetic susceptibility of Eu^{3+} compounds with temperature is specific compared to Gd^{3+} compounds. The magnetic susceptibility of Eu^{3+} compounds increases with decrease in temperature, reaches a temperature-independent constant value (over a temperature range) and then increases rapidly in the vicinity of 0–10 K. The magnetic susceptibility of EZT is measured in the temperature range 2–320 K. Fig. 9 shows the plot of χ^{-1} vs. temperature (T) of EZT. The variation of χ^{-1} with T can be divided in to three temperature zones viz: (i) 150–320 K, (ii) 25–150 K and (iii) 2–25 K. In the 150–320 K zone, the χ^{-1} decreases linearly with decrease in the temperature. χ^{-1} also decreases with decrease in temperature in the region 25–150 K but the slope is different (less). The decrease in the χ^{-1} in the temperature region 2–25 K is very rapid. The variation of χ^{-1} with T of EZT in the 150–320 K zone can be fitted to the Curie–Weiss type equation

$$\chi^{-1}=\frac{T}{C}-\frac{\theta}{C} \tag{3}$$

where θ is the Weiss constant. A good fit is obtained with slope and intercept as 0.377 and 88, respectively (Fig. 9). The effective magnetic moment estimated from, $\mu_{eff}=2.827(\chi T)^{1/2}$ at 300 K is found to be 3.49 BM which is comparable to free ion value of 3.58 BM.

The variation of χ^{-1} with temperature in the region II (25–150 K) does not follow the Curie–Weiss law. Unlike in other systems of Eu^{3+}, EZT does not exhibit temperature independent zone [34]. Although crystal field interactions are responsible for variation of χ^{-1} with temperature from 25 to 300 K, the same cannot be attributed to variation of χ^{-1} below 5 K. The dipolar and/or exchange interactions may be responsible for steep fall in χ^{-1} with decrease in temperature in the 0–5 K region. To get an estimation of nearest neighbor interactions (J_{nn}) and dipolar interactions (D_{nn}), the susceptibility data in the temperature region 0–5 K is fitted with high temperature series expansion equation of χ [15]. According to Ref. [5],

$$\chi=C\left[\left(\frac{1}{T}\right)+\left(\frac{\theta_{cw}}{T^2}\right)\right] \tag{4}$$

where C and θ_{cw} are the Curie constant and the Curie–Weiss constant, respectively. C and θ_{cw} are given by

$$C=\frac{N\mu_{eff}^2}{3k} \tag{5}$$

$$\theta_{cw}=z\frac{S(S+1)J_{nn}}{3} \tag{6}$$

where N is the Avagadro number, k is the Boltzmann constant, μ_{eff} is the effective magnetic moment (in BM) and z is the nearest neighbor and S = spin of Eu^{3+}. A plot of χT vs. $1/T$ for EZT is shown in Fig. 10. From the linear part of this curve, the C and θ_{cw} were found to be 0.0971 emu K/mol $EuZr_{0.5}Ti_{0.5}O_{3.5}$ and −1.827 K, respectively. From the slope and intercept values, μ_{eff} and $S(S+1)J_{nn}$ are found to be 0.88 and −0.913 BM, respectively. Raju et al. have defined classical nearest neighbor exchange (J^{cl}) and dipolar interactions (D_{nn}) as [35]

$$J^{cl}=S(S+1)J_{nn} \tag{7}$$

$$D_{nn}=\frac{\mu_{eff}^2\mu_0}{\{4\pi(a_0/\sqrt{8})^3\}} \tag{8}$$

where μ_0 is the magnetic permeability and a_0 is the unit cell length of pyrochlore lattice. In the present investigation for EZT system J^{cl} and D_{nn} are found to be −0.913 and 0.01 K, respectively. Thus near-neighbor exchange interactions (J^{cl}) are significant in EZT compared to

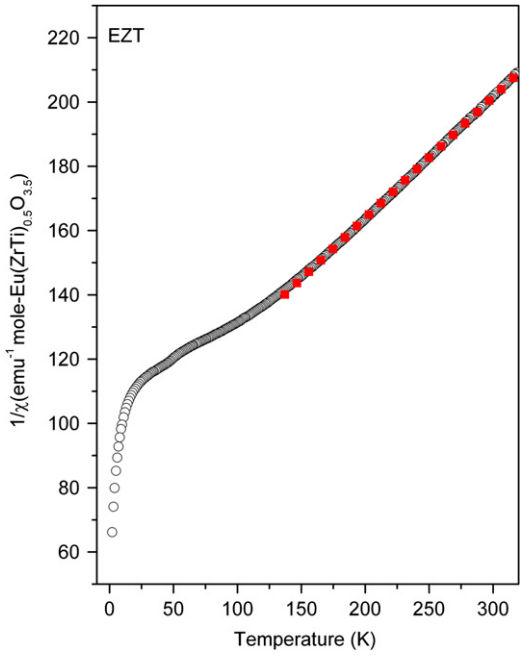

Fig. 9. Reciprocal magnetic susceptibility vs. temperature of EZT.

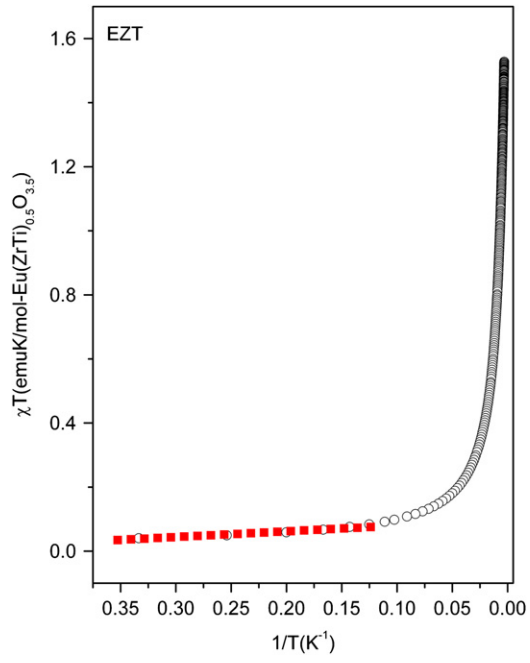

Fig. 10. χT vs. $1/T$ plot of EZT.

dipolar interactions. The similar observations are made in $Eu_2Ti_2O_7$ [34] and $Yb_2Ti_2O_7$ [8].

The geometrical frustration of spin in pyrochlore lattice is reported to be responsible [33] for magnetic ordering in these compounds. Nd, Gd and Sm compounds show long range ordering. A similar effect may also be present in Dy compounds. Doping of Zr in these compounds may change the geometrical spin frustration and range of ordering of spins in these compounds. The Raman spectra are generally related to moment of oxygen vibrational modes. Hence, the Raman spectra will have different modes of vibrations due to Ln–O, O–O and O–Ti–O vibrations. The disorder in the structure may be due to presence of rare earth ions in various environments. Zr doping in the place of Ti also affects O–Ti–O vibrational modes.

3.6. X-ray photoelectron spectroscopy

The X-ray photoelectron spectra of LZT, EZT, DZT and GZT are shown in Fig. 11. These spectra exhibit characteristic Ln 3*d*, Zr 3*d*, Ti 2*p* and O1*s* peaks. The 3*d* peak of lanthanide splits into $3d_{5/2}$ and $3d_{3/2}$ due to spin–orbit coupling, which varies from ~17 eV for La to ~37 eV for Dy. In the case of LZT, the La 3*d* profiles exhibit asymmetric peaks at 839 and 856 eV which are assigned to $3d_{5/2}$ and $3d_{3/2}$ levels of La^{3+}. Each asymmetric peak having shoulder on the low binding energy side is gauss fitted to locate the exact positions of the peaks. The less intense peaks, called satellite peaks, are separated by 3.0 eV from $3d_{5/2}$ and $3d_{3/2}$ main peaks. Such broad peaks with large FWHM were attributed to (a) a combination of life time effects and the exchange interaction between the 3*d* hole and partially filled 4*f* shell of Ln^{3+} ion [11,36] or (b) oxidized nature of rare earth atoms [37]. According to process (a), the less intense satellites and more intense main 3*d* peaks are ascribed to "well screened" $3d^9,\ldots,4f^{n+1}$ and "poorly screened" $3d^9,\ldots,4f^n$ configurations, respectively. Hillerbrecht and Fuggle have interpreted the observation of satellite peaks in the XPS spectra of lanthanide compounds due to "degree of mixing" (or hybridization) of 4*f* levels with extended conduction band states in $LnPd_3$ (Ln = La, Ce, Pr, Nd and Sm). It is noticed that the satellite peaks are well separated from main 3*d* peaks in the case of $LaPd_3$ while in $SmPd_3$ significant satellite peaks were not observed [11]. Based on the XPS spectra of these compounds, they have concluded that the degree of mixing decreases in the order La > Ce > Pr > Nd > Sm. The degree of mixing is dependent on the radial extension of 4*f* levels and the energy separation of dominant f^n and f^{n+1} multiplets. It was estimated that the energy difference between f^n and f^{n+1} states was found to increase from La (minimum) to Dy (maximum) [11]. According to process (b), the line shape of core-level lines is very sensitive to chemical environment/oxidation state of the core ionized atom [37]. In the present investigation, the observation satellite peaks only in the LZT sample can be attributed to degree of mixing of 4*f* levels. For the heavier rare earths (Eu, Gd and Dy) the mixing of 4*f* configuration is negligible and hence the satellite peaks are absent in EZT, DZT and GZT. The Zr $3d_{5/2}$ and $3d_{3/2}$ peaks were observed at 182 and 184 eV, respectively, and spin–orbit coupling (Δ) was found to be 2 eV. Similarly, the Ti $2p_{3/2}$ and $2p_{1/2}$ peaks were observed at 458.7 and 464.5 eV, respectively, resulting a spin–orbit coupling (Δ) of 5.8 eV which is comparable to that observed in related systems [38]. The O1*s* XPS peaks of LZT (533.1, 530.6 eV), DZT (532.2, 529.8 eV) and GZT (531.4, 529.4 eV) can be fitted into two Gaussians while the XPS of EZT (532.2, 530.8 and 529 eV) can be decomposed into three Gaussians (the values given in parenthesis indicate the positions of Gaussians). Chen et al. have also observed two components for O1*s* in $Gd_2Ti_2O_7$ which merged in to one when Ti (25–75%) was replaced by Zr [20]. In similar systems, Nd_2ZrTiO_7 and Sm_2ZrTiO_7, however, only one component was observed [22]. Nevertheless, site selective near edge X-ray absorption fine structure (NEXAFS) and XPS studies on $Gd_2Ti_2O_7$

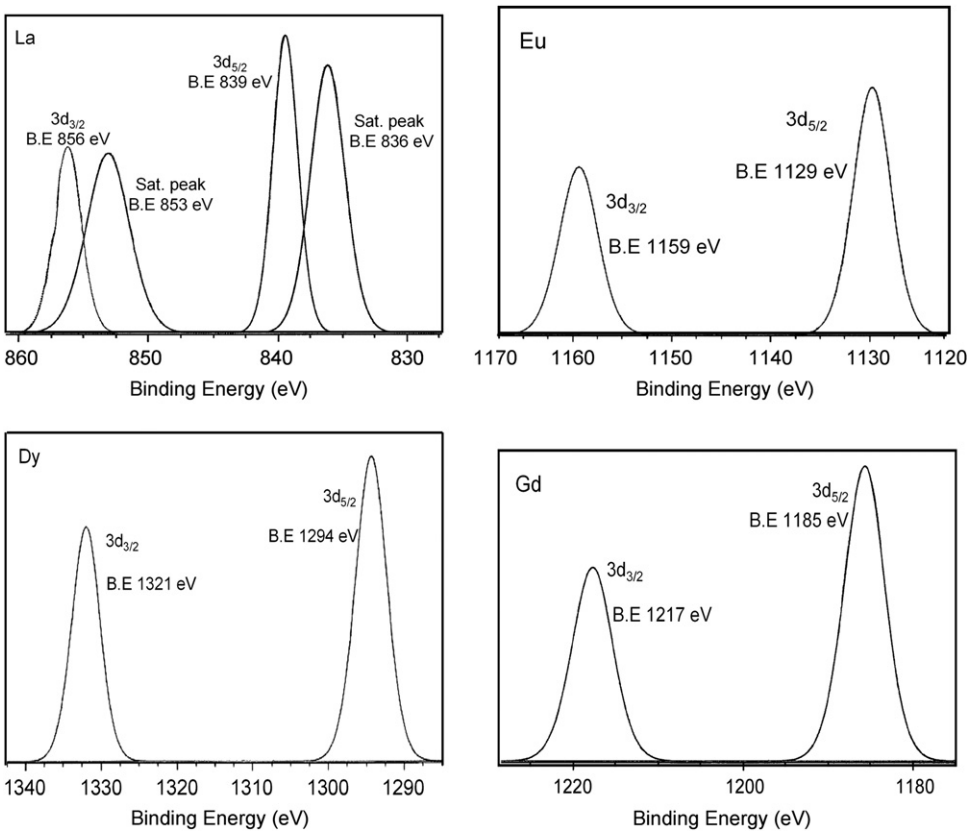

Fig. 11. XPS spectra of LZT, EZT, DZT and GZT.

single crystal have shown that the discrepancies observed by Chen et al. result from charging effects and surface contamination [39]. In the present investigation, the observation of multi components may be due to charging effects during the XPS and surface contamination.

4. Conclusions

Bulk and nanosized pyrochlores of composition Ln_2ZrTiO_7 (Ln=La, Eu, Dy and Gd) are prepared by the sol–gel synthesis employing peroxo titanium complex precursor and characterized by XRD, Raman and XPS. The Raman spectra of LZT and EZT gave characteristic bands corresponding to "ordered pyrochlore" structure while DZT gave a broad Raman spectrum corresponding to "weakly ordered pyrochlore". The magnetic susceptibility of GZT follows the Curie law in the temperatures range 2–320 K. The room temperature ESR spectrum of GZT gave a broad signal with g=2.05. The effective magnetic moment of GZT, calculated from the slope of χ^{-1} vs. T plot and ESR spectrum is found to be 7.6 and 8.1 BM, respectively, which is comparable to the free ion value of 7.94 BM expected for $4f^7$ configuration. The variation of χ with temperature of SZT follows the intermediate formula. The effective magnetic moment of SZT at 300 K is found to be 0.768 BM, which is smaller than the free ion moment of 1.3–1.4 BM. This may be due to the crystal field effects. The variation of χ^{-1} with temperature of EZT follows the Curie–Weiss law in the temperature region 150–320 K. The effective magnetic moment for EZT at 300 K is found to be 3.49 BM which is comparable to free ion value of 3.58 BM. The decrease in χ^{-1} with the temperature for EZT from 25 to 2 K is very rapid. The dipolar and/or exchange interactions may be responsible for steep fall in χ^{-1} with decrease in temperature in this region. The near-neighbor exchange interactions ($J^{cl}=-0.91$ K) are significant in EZT compared to dipolar interactions (D_{nn}=0.01 K). The XPS spectra of all the samples gave characteristic peaks corresponding to Ln, Ti, Zr and O. The XPS spectra of LZT gave satellite peaks for La 3d levels which are absent in EZT, DZT and GZT. This is attributed to the degree of mixing of 4f levels in the LZT and insignificant mixing of these levels in the EZT, DZT and GZT.

Acknowledgments

This work was supported by University Grants Commission, New Delhi under Grant no: 37-288/2009 (SR). The authors (S.A & M.K) wish to acknowledge the DST and UGC for the financial support to CHPR. One of us (BVK) thanks to the Council of Scientific and Industrial Research, New Delhi for the award of Senior Research Fellowship (CSIR-SRF).

References

[1] M.A. Subramanian, G. Aravamudan, G.V.Subba Rao, Oxide pyrochlores—a review, Prog. Solid State Chem. 15 (1983) 55–143.
[2] B.P. Mandal, N. Garg, S.M. Sharma, A.K. Tyagi, J. Solid State Chem. 179 (2006) 1990–1994.
[3] W.J. Weber, R.C. Ewing, Science 289 (2000) 2051.
[4] A.A. Digeos, J.A. Valdez, K.E. Sickafus, S. Atiq, R.W. Grimes, A.R. Boccaccini, J. Mater. Sci. 38 (2003) 1597.
[5] Y. Ji, J.A. Kilner, M.F. Carolan, Solid State Ionics 176 (2005) 937–943.
[6] J.M. Sohn, M.R. Kim, S.I. Woo, Catal. Today 83 (2003) 289–297.
[7] V.V. Kharton, E.N. Naumovich, A.V. Nikolaev, J. Membr. Sci. 111 (1996) 149–157.
[8] B.J. Wuensch, K.W. Eberman, C. Heremans, E.M. Ku, P. Onnerud, E.M.E. Yeo, S.M. Haile, J.K. Stalick, J.D. Jorgensen, Solid State Ionics 129 (2000) 111–133.
[9] P.K. Moon, H.L. Tuller, Solid State Ionics 28–30 (1988) 470–474.
[10] P.K. Moon, H.L. Tuller, Sensors Actuators B 1 (1990) 199–202.
[11] F.U. Hillerbrecht, F.J. Fuggle, Phys. Rev. B 25 (1982) 3550–3556.
[12] L.M. Falicov, Valence Fluctuations in Solids, in: M.B. Hanke, W. Maple (Eds.), North-Holland, Amsterdam, 1981, 487 pp.
[13] M.J. Harris, S.T. Bramwell, D.F. McMorrow, T. Zeiske, K.W. Godfrey, Phys. Rev. Lett. 79 (1997) 2554–2557.
[14] A.P. Ramirez, A. Hayashi, R.J. Cava, R. Siddharthan, B.S. Shastry, Nature 399 (1999) 333.
[15] M.J.P. Gingras, B.C. denHertog, M. Faucher, J.S. Gardner, S.R. Dunsiger, L.J. Chang, B.D. Gaulin, N.P. Raju, J.E. Greedan, Phys. Rev. B 62 (2000) 6496–6511.
[16] J.D.M. Champion, M.J. Harris, P.C.W. Holdsworth, A.S. Wills, G. Balakrishnan, S.T. Bramwell, E. Cizmar, T. Fennell, J.S. Gardner, J. Lago, D.F. McMorrow, M. Orendac, A. Orendacova, D.McK. Paul, R.I. Smith, M.T.F. Telling, A. Wildes, Phys. Rev. B 68 (2003) 020401.
[17] J.A. Hodges, P. Bonville, A. Forget, A. Yaouanc, P. Dalmas de Réotier, G. André, M. Rams, K. Królas, C. Ritter, P.C.M. Gubbens, C.T. Kaiser, P.J.C. King, C. Baines, Phys. Rev. Lett. 88 (2002) 077204.
[18] J. Yamaura, Y. Muraoka, F. Sakai, Z. Hiroi, J. Phys. Chem. Solids 63 (2002) 1027.
[19] I. Mirebeau, I.N. Goncharenko, P. Cadavez-Peres, S.T. Bramwell, M.J.P. Gingras, J.S. Gardner, Nature 420 (2002) 54.
[20] J. Chen, J. Lian, L.M. Wang, R.C. Ewing, R.G. Wang, W. Pan, Phys. Rev. Lett. 88 (2001) 105901.
[21] K.J. Moreno, M.A. Guevara-Liceaga, A.F. Fuentes, J. Garcıa-Barriocanal, C. Leon, J. Santamaria, J. Solid State Chem. 179 (2006) 928–934.
[22] B. Vijaya Kumar, V. Radha, G. Prasad, B. Sreedhar, K. Ravikumar, M. Vithal, Ceram. Int. 36 (2010) 1347–1355.
[23] B.P. Mandal, A.K. Tyagi, Mater. Sci. Eng. B 136 (2007) 46–49.
[24] L. Zhang, H. Zhong, W. Zhang, L. Lu, X. Yang, X. Wang, J. Alloys Compd. 463 (2008) 466–470.
[25] J.Y. Li, H. Dai, Q. Li, X.H. Zhong, X.F. Ma, J. Meng, X.Q. Cao, Mater. Sci. Eng. B 133 (2006) 209–212.
[26] S.J. Dickson, K.D. Hawkings, T.J. White, J. Solid State Chem. 82 (1986) 146–150.
[27] H.C. Gupta, S. Brown, N. Rani, V.B. Gohel, J. Raman Spectrosc. 32 (2001) 41–44.
[28] N.J. Hess, B.D. Begg, S.D. Conradson, D.E. McCready, P.L. Gassman, W.J. Weber, J. Phys. Chem. B 106 (2002) 4663–4677.
[29] H. Tang, K. Prasad, R. Sanjines, P.E. Schmid, F. Levy, J. Appl. Phys. 75 (1994) 2042.
[30] K. Tezuka, Y. Hinatsu, N.M. Masaki, M. Saeki, J. Solid State Chem. 138 (1998) 342–346.
[31] K. Koteswara Rao, M. Vithal, D. Ravinder, J. Magn. Magn. Mater. 253 (2002) 65–71.
[32] J.H. VanVleck, The Theory of Electric and Magnetic Susceptibilities, Oxford University Press, London, 1965.
[33] S. Singh, S. Saha, S.K. Dhar, R. Suryanarayanan, A.K. Sood, A. Revcolevschi, Phys. Rev. B 77 (2008) 054408.
[34] P. Dasgupta, Y.M. Jana, A. Nag Chattopadhyay, R. Higashinaka, Y. Maeno, D. Ghosh, J. Phys. Chem. Solids 68 (2007) 347–354.
[35] N.P. Raju, M. Dion, M.J.P. Gingras, T.E. Mason, J.E. Greedon, Phys. Rev. B 59 (1999) 14489–14498.
[36] J.C. Fuggle, S.F. Alvarado, Phys. Rev. A 22 (1980) 1615–1624.
[37] J.C. Fuggle, M. Campagna, Z. Zolnierek, R. Lasser, A. Platau, Phys. Rev. Lett. 45 (1980) 1597–1600.
[38] J. Wang, Z.G. Wu, X.M. Yuan, S.R. Jiang, P.X. Yan, Mater. Chem. Phys. 88 (2004) 77–83.
[39] P. Nachimuthu, S. Thevuthasan, E.M. Adams, W.J. Weber, B.D. Begg, B.S. Mun, D.K. Shuh, D.W. Lindle, E.M. Gullikson, R.C.C. Perera, J. Phys. Chem. B 109 (2005) 1337–1339.